Int J Adv Manuf Technol (2014) 71:33–45
DOI 10.1007/s00170-013-5449-0

ORIGINAL ARTICLE

Multi-material metallic structure fabrication using electron beam melting

Cesar A. Terrazas · Sara M. Gaytan · Emmanuel Rodriguez · David Espalin · Lawrence E. Murr · Francisco Medina · Ryan B. Wicker

Received: 19 July 2013 / Accepted: 15 October 2013 / Published online: 19 November 2013

Abstract The fabrication of multi-material structures using Ti–6Al–4V and copper was explored with the additive manufacturing (AM) technology of electron beam melting (EBM). A new method was developed that included multiple build sequences to accommodate both materials. The process was enabled by machining a start plate so that the parts built with the first material could be press fit into the plate, providing a flat surface on which the second material fabrication would occur. This method provided the ability to fabricate simple multiple metallic material components built in the Z and X directions [1]. Registration of the electron beam was performed manually resulting in slight misalignment for the shift of diameters of specimens built in the Z direction, and along the width and length for specimens built in the X direction. Microstructures observed and hardness values measured for copper and Ti–6Al–4V were different to those observed in normally fabricated EBM parts. These observations might be explained by the different processing conditions required for multi-material fabrication in contrast to the regular EBM process where parts are built in a single machine run. The hardness profiles for as-fabricated and HIPed multi-material parts depicted an increase in hardness for both materials close to the interface with values leveling off to those of single material EBM fabricated parts as measurements proceeded away from the interface. As the benefits of EBM processing are exploited, the method introduced in this research can have profound implications in many technological applications including metal extraction, energy production and for the repair of metallic components.

Keywords Additive manufacturing · Multi-material fabrication · Copper · Titanium · Ti-6Al-4V · EBM

C. A. Terrazas (✉) · S. M. Gaytan · E. Rodriguez · D. Espalin · F. Medina · R. B. Wicker
W. M. Keck Center for 3D Innovation, University of Texas at El Paso, El Paso, TX, USA
e-mail: caterrazas2@miners.utep.edu

L. E. Murr
Metallurgical and Materials Engineering Department, University of Texas at El Paso, El Paso, USA

1 Introduction

Additive manufacturing (AM) comprises a group of technologies within the field of manufacturing that allow for the automated fabrication of three-dimensional (3D) structures from computer models in a layer-by-layer fashion [1, 2]. These technologies provide certain advantages compared to traditional manufacturing such as injection molding, because AM enables, for example, fabrication of complex geometries with internal features and functional parts and assemblies without the expense of tooling. Extensive research with the use of AM technologies has provided means for the fabrication of components that are made of a wide variety of materials including polymers, metals, ceramics, and composites, which have found applications in many industries such as automotive, biomedical, electronics and aerospace. Interest in the fabrication of multi-material parts that are able to provide spatial control over specific properties has helped accelerate the research in AM technologies. The ability to control material placement and structure creation for fabrication of multi-material parts has the potential to revolutionize engineering design and manufacture.

Fabrication of structures exhibiting multiple materials has been achieved with the use of several AM technologies employing a variety of materials. For instance, the vat photopolymerization process, stereolithography (SL), has been used extensively for multiple material part fabrication [2]. The development of a multi-material SL machine enabled the fabrication of functional multiple material parts using various photopolymerizable resins [3]. Despite several issues

identified in this study such as laser shadowing, volume entrapment and surface tension mismatch among the resins, the process was successfully used to fabricate complex multi-material models that could be employed for illustrative purposes [4]. Detailed structures created by combining commercial resin materials across or in single layers were also fabricated by a micro stereolithography (μSL) system using a syringe pump for material dispensing. Even though the study acknowledged the need for correcting dimensional errors resulting from surface tension forces and UV overcure, it demonstrated the ability to create micron-size multi-material components [5]. Similar work with SL and the implementation of a self-aligning mini-vat provided means for fabricating 3D multi-material structures out of bioactive and biocompatible hydrogel photopolymers exhibiting features as small as 500 μm which could be used in tissue engineering applications [6]. Finally, integration of a SL machine with a direct print (DP) system allowed for fabrication of monolithic 3D structures with embedded electronics in a single manufacturing setup. The developed hybrid process required manual operation of sub-processes which presented further opportunities for its automation and optimization but nonetheless demonstrated a practical application for multi-material, multi-technology fabrication using AM [7].

Another AM process that has been used in multi-material fabrication is the powder bed fusion process known as laser sintering (LS). The fabrication of small multi-material (metal–insulator–metal) micro-electronic components such as capacitors and spiral inductors with overpasses was achieved by sintering layers of conductive and dielectric inks on top of soda-lime substrates using this technology [8]. The process provided the advantage of reducing the high temperature post-processing usually needed to functionalize such micro-electronics but required balancing the laser power to achieve adhesion of the inks without damaging the substrate by overheating. LS has also been employed in the creation of functionally graded materials (FGM) using Nylon-11 and silica nanoparticles exhibiting a one dimensional material gradient [9]. The method was successfully employed in the fabrication of near theoretical density FGM parts with up to 6 % volume fraction of silica nanoparticles using a single, uninterrupted run. The attempt to fabricate structures with 10 % volume content of silica yielded un-sintered layers that did not attach to the building substrate resulting in failed components.

Fabrication of multi-material components using metallic materials is most representative of studies done with the directed energy deposition process known as laser-engineered net shaping (LENS™). Early work with this process resulted in dense multi-material parts with both graded and layered structures using combinations of metals that included Inconel 690, stainless steel 316 and tool steel MM10 [10]. More recently, LENS™ has been utilized to fabricate functionally graded coatings of Co–Cr–Mo on Ti–6Al–4V structures that were crack free for compositions up to 86 % Co–Cr–Mo. The coatings provided higher wear resistance and surface hardness without the presence of intermetallic phases in the transition zone while enhancing biocompatibility, compared to 100 % Co–Cr–Mo components, as demonstrated by in vitro cell seeding experiments [11]. In a similar fashion, the yttria-stabilized zirconia (YSZ) ceramic was deposited on 316 L stainless steel components to serve as a graded thermal barrier coating (TBC) using LENS™. Researchers found sound metallurgical bonding of the materials using these graded coatings–compared with conventional homogeneous coatings–which even though were not crack-free resulted in better compliance and reduction of interfacial thermal stresses improving the service performance of the TBCs [12].

Finally, the sheet lamination process known as ultrasonic consolidation (UC), a commercial process for solid state joining of materials, has also been successfully employed in the fabrication of multiple material metallic structures by joining of several laminas or foils of various materials. By means of this technique, the fabrication of multi-material parts with discrete material regions using 3003-H18 aluminum alloy as a matrix and the commercially available metal matrix composite MetPreg® and unalloyed titanium as fillers, has been reported [13]. This research achieved the fabrication of minimum weight structures by layering the different materials resulting in parts that exceeded the carrying capacity of similar matrix only components.

The joining of dissimilar metallic materials has long been recognized as having practical applications across multiple areas. Several metallic material combinations such as Ni-based superalloys joined to stainless steel or niobium (Nb) coupled to copper (Cu) have been listed, and these materials, in principle, could be joined by the process of electron beam welding (EBW). Potential applications of these material combinations include power generation systems, electronic and electromagnetic devices, and aerospace and marine components [14]. Similarly, more recent work using UC of metals provided potential applications of multi-material functional structures which included protective coatings for corrosion or wear resistance, shielding for radiation, as well as for use in the fabrication of complex insulator–conductor materials which might be suitable for use in industrial machinery and the nuclear industry [15]. The development of technologies that harness the potential for multi-material metallic fabrication can provide higher flexibility in the design stages while also allowing tailoring specific properties in the fabricated components depending on the required application.

As described above, fabrication of multi-material structures (metallic and non-metallic) has been performed with several AM technologies. However, fabrication of multi-material metallic parts has not been reported, or at least identified by the authors, with the use of the powder bed fusion process known as electron beam melting (EBM) most likely due to the many issues associated with achieving the EBM. For example, the

EBM system is designed to work with only one material per build. Even though there are two containers for metal powder located at each side of the build envelope, the system rakes from both directions; thus, the introduction of two powder materials will inherently cause their mixing. Also, EBM does not allow easy access to the build chamber during fabrication since the system operates under vacuum. The evacuated system generally makes this process not feasible for material switching during fabrication. If a material changeover is desired, a complete cool down of the system is needed prior to gaining access to the build envelope. Once the machine is opened, it needs extensive cleaning of all the internal components within the build chamber before introducing a new material to avoid material contamination. If a new material is placed in the machine, the process must be restarted, requiring the build chamber to be evacuated once again and preheating of the material already placed in the build volume to a temperature typically close to half of the melt temperature of the material being processed, which would be the new material in this case. This scenario presents complications that are intrinsic to the materials used in the process as each requires specific processing parameters. That is, it may be impossible to process several materials if they have widely different melting points. Further, differences in coefficients of thermal expansion can also lead to the development of thermal stresses in fabricated parts making them more susceptible to failure. Finally, there are complications associated with the build process that makes accurate registration of parts between build sequences difficult.

Despite these complications, fabrication of multi-material structures using EBM could, in principle, provide advantages when compared to other AM technologies. The required vacuum provides high energy efficiency while allowing the processing of reactive metals and alloys, such as Ti–6Al–4V, which would otherwise be susceptible to high levels of oxidation. Further, microstructures obtained from EBM fabricated components exhibit improved mechanical properties similar to those of the wrought material. For example, Murr et al. [16] found Ti–6Al–4V EBM fabricated parts to have higher values of elongation, yield stress (YS) and ultimate tensile strength (UTS) when compared to Grade 5 nominal Ti–6Al–4V. Similarly, the microstructure of copper components fabricated by EBM, which exhibited elongated grains as well as precipitate-dislocation features, was correlated with a hardness increase of 54 % when compared to copper in the precursor powder state [17]. Another advantage of EBM results from the part under fabrication being maintained at elevated temperatures (as mentioned previously, approximately half of the melting temperature of the material), minimizing the occurrence of thermally induced residual stresses, segregation and the appearance of non-equilibrium phases in the finished parts. In other metal based AM powder bed fusion technologies such as selective laser melting (SLM), the appearance of the above issues has been associated with thermal gradients during fabrication, negatively impacting the material properties [18]. In multi-material part fabrication, thermal stresses at material interfaces might be minimized by EBM due to temperature control, although not completely eliminated because of the mismatch in the coefficient of thermal expansion of the dissimilar materials.

In this research, a method was developed that provided solutions to some of the complications for multi-material fabrication using EBM. This method was utilized to produce simple cylindrical multi-material parts, built with their longest axis in the Z and X directions, using discrete builds with pure copper and Ti–6Al–4V. Fabrication was enabled by the use of a mask plate with CNC-machined sections that allowed the parts built with the first material to be securely press fit into the plate, thus providing a flat surface on which the second material could be fabricated. A manual registration process was used to center the electron beam to the mask plate between the material changeover, and two build sequences (one for copper and one for Ti–6Al–4V) were used to build the multiple material parts in an Arcam A2 EBM system (Arcam AB, Sweden). Samples were successfully fabricated and characterization of the specimens suggested a sound metallurgical bond between copper and Ti–6Al–4V. Measurements taken in the vicinity of the interface of as-fabricated and HIPed samples indicated an increase of hardness in both the copper and Ti–6Al–4V sides. Starting at the interface and advancing in opposite directions into each material, hardness peaked close to the interface and slightly decreased to similar values as those previously reported for both EBM fabricated copper and Ti–6Al–4V. This preliminary study was carried out to demonstrate the feasibility of producing multi-material parts with this technology without modification to the EBM machine. The following sections describe the method developed for building out of multiple materials in EBM as well as the results from this study. The results obtained demonstrate the feasibility of using current EBM technology to fabricate multi-material components with discrete material regions. Because of the advantages offered through EBM processing, this technology may become very useful for repair of metallic components through extensions of the research presented here.

2 Materials and methods

2.1 Electron beam melting system

The major components of the Arcam A2 EBM system (Fig. 1) include the electron gun (1), magnetic lenses (2), powder contained in the hoppers (3), rake mechanism (4), and build table (6) that translates the work piece (5). Consolidation is achieved by melting and solidification of metal powder in a

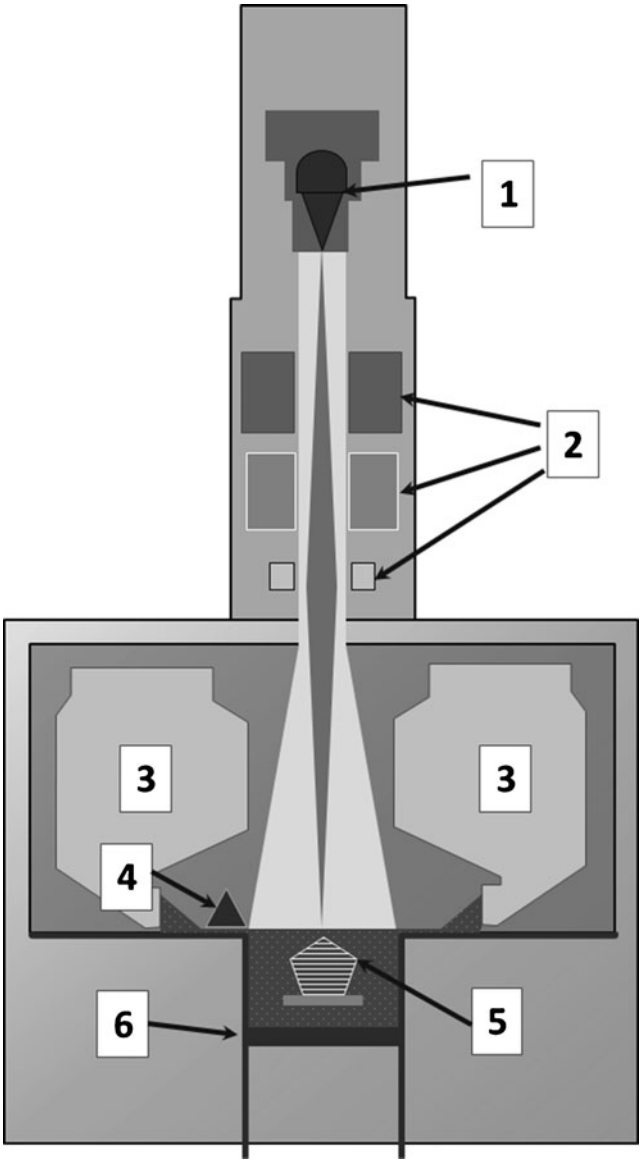

Fig. 1 Schematic of the Arcam EBM system with major components numbered

layer-by-layer fashion using a high energy electron beam operating at 60 keV. Magnetic lenses focus and scan the electron beam over the geometry in the current layer to melt the metal powder particles. The process is performed under vacuum (~10^{-4} Torr) to achieve transfer of the kinetic energy of the electron beam to the powder particles. In the standard configuration, a solid metal plate is utilized as the initial planar substrate for starting fabrication. The material for the start plate depends on the metal powder to be processed but a stainless steel plate is commonly employed. A component is built by the successive deposition of a fresh powder layer, the preheating of each powder layer, and the melting of the geometry indicated by the CAD model in the current slice. Typical layer thicknesses range from 70 to 200 μm. The metal powder flows by gravity out of containers (hoppers) located at each side of the rake mechanism. Once the fabrication is complete, helium is used to purge the build chamber that also assists in cooling of the part. Finally, the parts are extracted and post-processed using a powder recovery system (PRS) to remove any remaining sintered powder.

2.2 Material selection

The materials selected for fabrication were gas atomized Ti–6Al–4V ELI (Grade 23) (Arcam AB, Sweden) with a particle size range of 45–100 μm and 99.99 % pure copper (Sandvik AB, UK) with a measured particle size range of 45–125 μm. The coefficient of thermal expansion (Table 1) for these materials differ (Ti–6Al–4V with 8.6 μm/m°C [19], copper at 16.4 μm/m°C [20]), and this difference has been associated with the appearance of undesirable thermal stresses or the formation of brittle intermetallic phases upon joining of both materials [14]. Nevertheless, important technological innovations can be obtained from the combination of titanium and copper. For example, copper electroplated titanium wires have been investigated for use as strengthening components in superconductor magnets that provide high mechanical and thermal stability of titanium and the superior conductivity of copper [21]. Similarly, tubular copper–titanium joints formed by electrohydropulse have been fabricated to operate as cathode current leads in electrolyzers that are able to withstand a combination of harsh chemical environments and high temperatures [22, 23]. Commercial titanium-clad copper electrodes are available from Anomet Products Inc., USA for various industrial uses including electroplating, chemical processing and recovery of metals.

2.3 Multi-material part fabrication

As described previously, the Arcam A2 EBM system is designed to process only one material at a time. A method was implemented to fabricate multi-material parts using discrete runs of the EBM system. The process steps (Fig. 2) for this new method are (1) EBM fabrication and cleaning of bottom

Table 1 Mechanical and thermal properties for Ti–6Al–4V and copper at ambient temperature [19, 20]

	Ti–6Al–4V	Copper
Mechanical properties		
Hardness, Vickers	349	50
UTS (MPa)	900	210
Tensile strength (MPa)	830	33.3
Modulus of elasticity (GPa)	114	110
Thermal properties		
Linear CTE (μm/m °C)	8.6	16.4
Melting point/range (°C)	1,604–1,660	1,083

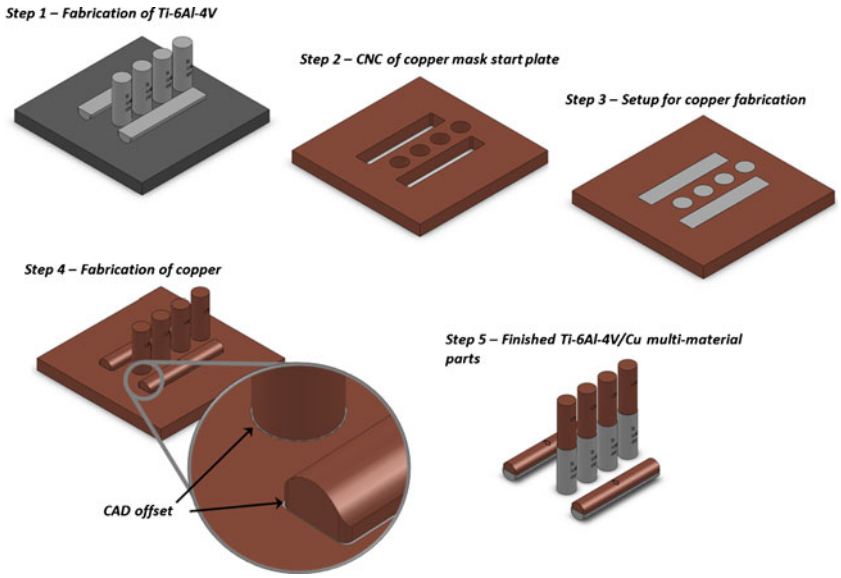

Fig. 2 Process followed in the fabrication of multi-material components using the EBM system

halves made of Ti–6Al–4V; (2) fabrication of copper mask plate using CNC machining; (3) setup of copper mask start plate with the inserted Ti–6Al–4V components fabricated in the first step; (4) EBM fabrication of upper halves using copper; and (5) cleanup of finished multi-material parts. Specifically, Step 1 consisted of fabricating the bottom halves of the components with their long axis in the *X* and *Z* directions and using the material with the highest melting temperature, Ti–6Al–4V. The traditional build sequence (build parameters, start plate, machine preparation, etc.) was used to build six Ti–6Al–4V parts. A total fabrication time of ~16 h was required for two half-cylinders with the long axis in the *X* direction and four in the *Z* direction. After fabrication, the system was allowed to cool after which the parts were removed from the powder bed and cleaned in the PRS. The time required for cleaning was ~20 min for all parts. Afterwards the EBM system was cleaned and the building material was changed from Ti–6Al–4V to copper. The Arcam A2 system including the chamber, vat, raking mechanism, hopper containers and heat shields, was cleaned to avoid contamination between the two build materials by dusting with compressed air and cleaning with isopropyl alcohol. The cleaning process took approximately 5 h.

Step 2 of the multi-material fabrication process consisted of CNC machining the openings in a stock copper piece to produce a copper mask start plate. The machined mask start plate enabled insertion and fixation of the Ti–6Al–4V components and provided a planar surface for fabrication with copper. In Step 3, the Ti–6Al–4V bottom halves were press fit into the machined openings of the mask plate, and the resulting assembly was manually positioned inside the build vat. The alignment process for the start plate inside the build vat was performed to achieve fabrication of copper over the Ti–6Al–4V parts as will be discussed in Section 2.6.

Fabrication of copper (Step 4) atop the Ti–6Al–4V inserts was carried out using a single run of the Arcam A2 for approximately ~10 h. Copper cylinder halves oriented in the *X* direction were 8 mm in height while the *Z* direction specimens had a height of 37 mm. At the end of fabrication, the machine was once again allowed to cool, and the multiple material parts consisting of copper atop of Ti–6Al–4V were removed from the mask start plate (Step 5). Removal of the sintered copper powder in the multi-material parts was done using a metal brush as a final post-processing step requiring ~1 h.

2.4 Mask plate fabrication

Starting with a stock copper rectangular bar, a section was cut to produce a plate with dimensions of 150 mm per side and 12.5 mm in thickness. A CNC Mini Mill 2 (HAAS Automatic Inc., USA) was used to machine openings into the plate. The openings were undersized compared to the dimensions of constructed Ti–6Al–4V parts. Five measurements were taken for each Ti–6Al–4V part, using a Mitutoyo digital caliper (Mitutoyo, America Corp., USA), and the average and standard deviation were calculated (Table 2). For cylinders built with their longest axis in the *Z* direction, diameter values were recorded along the length of the specimens in intervals of ~9 mm. Similarly, for half-cylinders built in the *X* direction, measurements of the width and length were recorded at distances ~2 mm apart from each other.

Based on the recorded measurements, the openings in the mask start plate were made with undersized dimensions of 13 μm and a tolerance of ±13 μm (0.0005 in. in all directions to obtain a press fit of the Ti–6Al–4V parts, as it is common practice in the fitting of machine alignment components such as metal dowel pins [24]. One of the circular openings in the

Table 2 Measurements of fabricated components (all units in mm)

Ti–6Al–4V										
Vertical cylinders	CAD	D1	D2	D3	D4	D5	Davg	StDev	Shrinkage	Shrink %
Specimen 1	16.51	16.33	16.30	16.28	16.31	16.44	16.33	0.06	0.18	1.08
Specimen 2	16.51	16.29	16.32	16.32	16.31	16.40	16.33	0.04	0.18	1.10
Specimen 3	16.51	16.51	16.50	16.29	16.35	16.39	16.38	0.10	0.13	0.77
Avg							16.35			0.98
Horizontal cylinders										
Width	CAD	W1	W2	W3	W4	W5	Wavg	StDev	Shrinkage	Shrink %
Specimen 1	16.51	16.23	16.24	16.22	16.28	16.40	16.27	0.07	0.24	1.43
Specimen 2	16.51	16.35	16.37	16.25	16.30	16.32	16.32	0.05	0.19	1.16
Avg							16.30			1.30
Length	CAD	L1	L2	L3	L4	L5	Lavg	StDev	Shrinkage	Shrink %
Specimen 1	90.00	89.13	89.50	88.90	90.10	88.83	89.29	0.52	0.71	0.79
Specimen 2	90.00	89.56	90.00	88.60	89.43	88.40	89.20	0.67	0.80	0.89
Avg							89.25			0.84
									Avg shrinkage %:	1.04 %
Copper										
Vertical Cylinders	CAD	D1	D2	D3	D4	D5	Davg	StDev	Shrinkage	Shrink %
Specimen 1	16.00	15.56	15.60	15.50	15.58	15.71	15.60	0.08	0.40	2.52
Specimen 2	16.00	15.80	15.85	15.75	15.74	15.67	15.76	0.07	0.24	1.49
Specimen 3	16.00	15.66	15.75	15.73	15.72	15.71	15.73	0.03	0.27	1.70
Avg							15.70			1.90
Horizontal cylinders										
Width	CAD	W1	W2	W3	W4	W5	Wavg	StDev	Shrinkage	Shrink %
Specimen 1	15.52	15.67	15.54	15.54	15.40	15.32	15.49	0.14	0.03	0.17
Specimen 2	15.52	15.41	15.46	15.35	15.44	15.36	15.40	0.05	0.12	0.75
Avg							15.45			0.46
Length	CAD	L1	L2	L3	L4	L5	Wavg	StDev	Shrinkage	Shrink %
Specimen 1	90.00	89.55	88.37	89.12	89.50	89.44	89.20	0.49	0.80	0.89
Specimen 2	90.00	89.90	88.75	89.26	88.87	89.45	89.25	0.46	0.75	0.84
Avg							89.22			0.87
									Avg shrinkage %:	1.08 %

mask plate was machined to coincide with the geometric center of the plate. This not only offered a fitting place for one of the inserts but also served as a reference for centering the electron beam during the setup. A schematic of the machined mask start plate is shown in Step 2 of Fig. 2.

2.5 Mask plate thermal expansion

One concern of the building process described in Section 2.3 was that the Ti–6Al–4V components would not remain fixed to the copper mask start plate during the copper build because there was a mismatch in coefficient of thermal expansion. Even though powder underneath the mask start plate provided support for the Ti–6Al–4V inserts, thermal expansion of the openings in the mask start plate could loosen the inserts, allowing them to move and preventing appropriate fabrication. An analysis was performed to calculate the clearances between the openings in the mask start plate and the inserts due to thermal expansion. Isotropy was assumed for the coefficients of thermal expansion for both materials (Table 1) and the following equation was used.

$$L_{\mathrm{f}} = L_0 * [1 + \alpha * (T_{\mathrm{f}} - T_0)]$$

The f and 0 sub-indices indicate final and initial states, respectively, for temperatures and linear dimensions. The thermal coefficient of linear expansion is denoted by α, the value T_0 was taken as the standard ambient temperature of 25 °C, and T_{f} was set as the pre-heat temperature for copper in EBM (550 °C, which is about half its melting point). Using this equation, thermal expansion values were calculated for different features in the copper mask plate and the Ti–6Al–4V inserts (Table 3). After thermal expansion, the maximum clearance (computed as the difference in the expanded

Table 3 Thermal expansion calculations

	Original dimensions (mm)			Expanded dimensions (mm)		
	Circular hole	Rectangular opening		Circular hole	Rectangular opening	
	Diameter	Length	Width	Diameter	Length	Width
Cu mask plate	16.34	89.24	16.29	16.48	90.01	16.43
Ti–6Al–4V insert	16.35	89.25	16.30	16.42	89.65	16.37

dimensions between the openings in the copper mask plate and the Ti–6Al–4V inserts) was calculated at ~350 μm along the length of a rectangular opening and ~55 μm for its width. For the diameter of a circular hole, the clearance was obtained as ~55 μm. Excluding the calculated clearance on the length, the dimensions after expansion still provided a slip fit–instead of the initially intended press fit–of the inserts (~50±13 μm [25], which — along with the support from the powder below the mask plate — was sufficient to anchor the inserts throughout the fabrication process.

2.6 Part registration

During the copper fabrication run, the copper mask plate (including fitted Ti–6Al–4V halves) was centered in the vat using a manual registration process. The plate was aligned by measuring equal distances along the plate edges to the walls of the vat using a standard scale (Luna AB, Sweden). The electron beam was placed at the center of the start plate represented by a small "X" that was marked into the surface of the Ti–6Al–4V insert located at the center of the mask plate. The aligned mask plate is shown in Fig. 3.

Anticipating possible misalignment of the mask start plate to be in the range from 0.5 to 1 mm in both *X* and *Y* directions, the CAD models for copper were undersized to keep all copper fabrication confined to the exposed surfaces of the Ti–6Al–4V inserts. Using the measured values of Ti–6Al–4V components as a reference (Table 2), the dimensions of the copper models were set at 16 mm for the diameter of vertical specimens and 15.5 and 89 mm for the respective width and length of horizontal specimens.

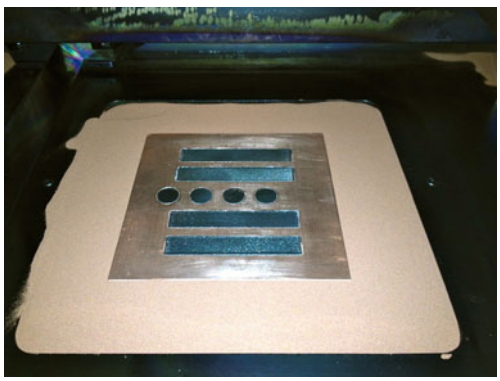

Fig. 3 Photograph of a copper mask start plate with Ti–6Al–4V inserts as the initial setup for multi-material fabrication

2.7 Hot isostatic pressing

Hot Isostatic pressing (HIPing) is a standard procedure carried out to increase the density and improve mechanical properties in metallic components fabricated from alloys including Ti–6Al–4V [26]. In this study, one multi-material vertical specimen was subjected to a HIPing cycle, which involved 2.25 h of heating to a temperature of 900± 4 °C under a pressure of 101.7±1.7 MPa. The HIPing cycle was also applicable for the copper without melting of the material. Sections from this specimen were used for metallographic observations, hardness measurements, and were compared to as-fabricated specimens.

2.8 Metallography

Metallographic sections were obtained from the fabricated components for characterization. Both types of specimens (horizontal and vertical cylinders) were sectioned to reveal the Ti–6Al–4V/copper interface. Cuts were made along a plane parallel to the build direction of approximately 7×7 mm of each material (Fig. 4). The sections were mounted, ground, polished and etched.

Given the multi-material nature of the fabricated parts, more than one etchant solution was required. Ti–6Al–4V was exposed for 10 s to an etchant prepared with 100 ml water, 2.5 ml hydrofluoric acid (HF) and 5 ml nitric acid

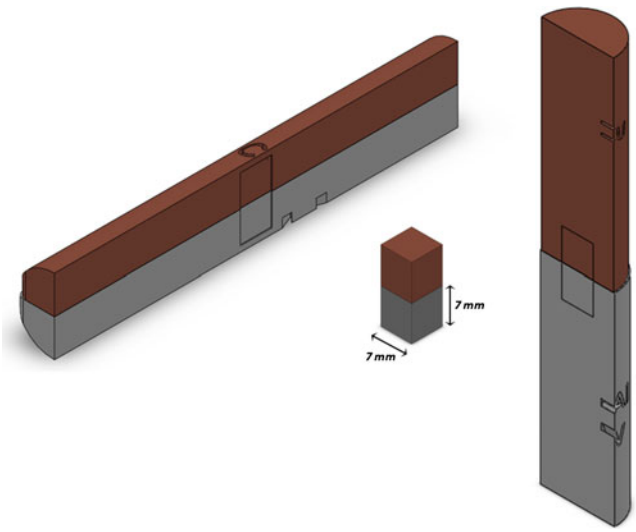

Fig. 4 Characteristic sections extracted from multi-material part

(HNO_3) [16]. Copper was etched for 5 s using a medium containing 100 ml of water, 8 ml sulfuric acid (H_2SO_4), 4 ml saturated sodium chloride (NaCl), and 2 g potassium dichromate ($K_2Cr_2O_7$) [17]. The etchants were applied using cotton swabs to the intended material. Following etching, samples were submerged in distilled water, rinsed with methanol, and dried by convection using a heat gun (Master Appliance Corp., USA). Prepared samples were observed using a Reichert MF4 A/M (Reichert, USA) optical microscope and a Hitachi S4800 (Hitachi, Japan) field emission scanning electron microscope (SEM) operating at a voltage of 20 kV.

2.9 Hardness testing

Vickers micro-indentation hardness testing was performed using a Struers Duramin-A300 tester (Struers A/S, Denmark) having a minimum indenter diagonal width of 20 μm and using a 100 g load. A grid of hardness measurements was recorded for each specimen. Twelve values were recorded at points distanced 1 mm apart along a straight line perpendicular to the interface starting on the copper side of the specimen and ending on the Ti–6Al–4V side. The process was repeated along five parallel lines separated by ~1 mm, thus covering a measurement grid area of approximately 60 mm^2. The average hardness was based on the five measurements taken at the same distance from the interface on the five parallel lines. Using this procedure a hardness profile was obtained for as-fabricated and HIPed specimens.

3 Results and discussion

3.1 Fabrication of multi-material specimens

The methodology described above was used to fabricate multiple material specimens using the EBM technology. Multiple material fabrication was performed in a straightforward manner without requiring modifications to the Arcam A2 system other than using the specific build parameters for the material in the machine and a material exchange process whenever a new build material was used. The process, which employed a single build run per material, has demonstrated the capability of joining dissimilar materials, which yielded specimens made of Ti–6Al–4V and pure copper (Fig. 5). Fabrication of several parts per build was possible by placement of several Ti–6Al–4V inserts in the mask start plate at once. For the parts shown in Fig. 5, a total of six specimens (two horizontal and four vertical cylinders) were built using Ti–6Al–4V and copper as the first and second build materials, respectively. The total fabrication time for these specimens was ~30 h, which included the intervals for the Ti–6Al–4V and copper builds (preparation, build, and part removal with cleaning) with the intermediate material exchange in between.

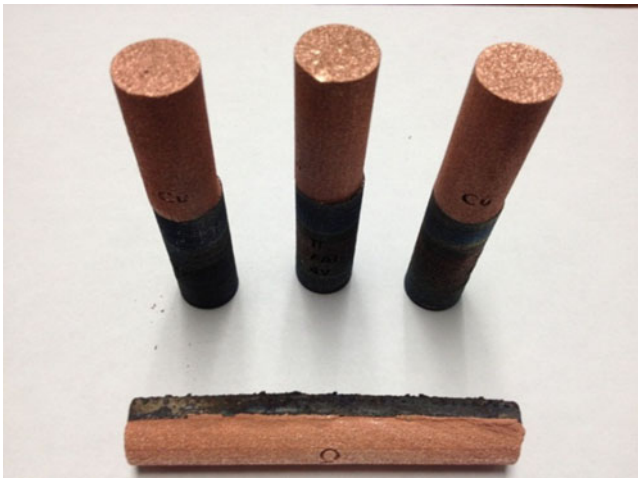

Fig. 5 Photographs of fabricated cylindrical Ti–6Al–4V — copper specimens with the long axis in the *X* and *Z* axes

The fabricated Ti–6Al–4V and copper specimens had a metal–metal bond which was apparent by the ability of both materials to remain joined after fabrication. The Ti–6Al–4V portion changed color in the finished multi-material part, which was indicative of oxidation in this material. In studies of emissivity of metals and metal oxides, it has been observed that metallic components processed in a vacuum environment undergo thermal oxidation when exposed to ambient conditions followed by reheating once again in vacuum [27].

3.2 Part registration

The measuring of the specimens revealed that part registration was deficient since the fabricated copper showed misalignment compared to the CAD models. As explained in Section 2.6, the use of undersized dimensions for the copper models provided an initial offset for ensuring fabrication only atop the available surfaces of the Ti–6Al–4V inserts. These calculated values (Table 4), denoted as "CAD offset", served as a baseline for evaluating misalignment by comparing against measurements taken at specific locations in the fabricated copper (Fig. 6), and that were referred to as "Part offset". Misalignment values were determined by subtracting the part offset values from direct measurements in the specimens and averaged (Table 5). For vertical specimens, the shift of the copper cylinder center from that of the Ti–6Al–4V cylinder

Table 4 CAD and part offset (μm)

	CAD offset	Part offset
Vertical (*Z*) cylinders (shift in diameters)	255	326
Horizontal (*X*) cylinders (shift in width)	495	424
Horizontal (*X*) cylinders (shift in length)	0	12

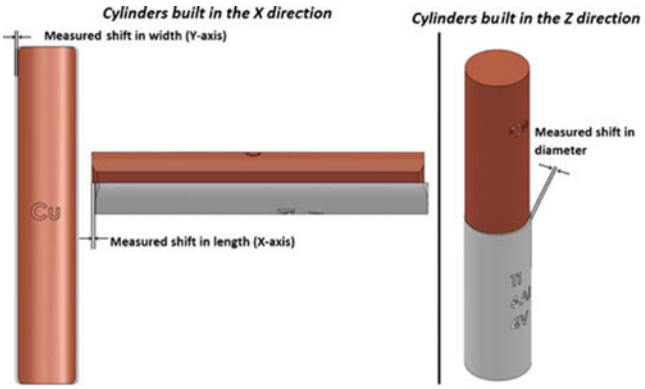

Fig. 6 Location where measured shifts were taken in *X* and *Y* cylinders to evaluate misalignment

was denoted as the misalignment and it averaged ~70 μm. For horizontal specimens, the misalignment along the width or Y direction was ~65 and ~325 μm in length or *X* direction.

Improved registration of parts is required to optimize the EBM multi-material fabrication method. A platform for holding the mask start plate is being developed to provide registration in the *X* and *Y* axes between runs. Acting as a spacer to the walls of the vat, this platform should provide alignment tolerances that approximate the ±0.2mm resolution of the EBM process from layer to layer [28]. Furthermore, a procedure for centering the electron beam could also be used by machining sub-millimeter orifices in the corners and midway along the edges of the mask start plate to serve as references for positioning of the beam during the setup.

Table 5 Measured misalignment values

Vertical (*Z*) cylinders				
	Diameter (Ti–6Al–4V) (mm)	Diameter (Cu) (mm)	Measured shift (μm)	Misalignment[a] (μm)
Cylinder 1	16.32	15.66	331	4.67
Cylinder 2	16.38	15.68	377	51.3
Cylinder 3	16.40	15.59	481	155
StDev	0.04	0.05		
		Average (μm)	396	70
Horizontal (*X*) cylinders				
	Misalignment in *Y* direction (width)		Misalignment in *X* direction (length)	
	Measured shift (μm)	Misalignment[b] (μm)	Measured shift (μm)	Misalignment[b] (μm)
Cylinder 1	494	70.5	311	299
Cylinder 2	369	54.5	362	350
StDev	88.4		36.1	
	Average (μm)	62.5	Average (μm)	324

[a] Misalignment calculated as the shift in the center of the copper cylinder from the center of the Ti–6Al–4V cylinder

[b] Misalignment calculated as measured shifts in width and length

3.3 Microstructure

The micrographs for as-fabricated specimens revealed the microstructures at (a) the bonded interface, and at distances ~5 mm within (b) Ti–6Al–4V and (c) copper (Fig. 7). A regular acicular or elongated grain structure was observed in the Ti–6Al–4V side corresponding to α and β phases [16]. The average grain width of the α phase for as-fabricated EBM Ti–6Al–4V was 0.69 and 3.71 μm for the HIPed specimen. By comparison, an average grain width for the α phase of 3.2 μm has been previously reported for as-fabricated EBM Ti–6Al–4V [16]. No information is available in literature regarding microstructures of EBM Ti–6Al–4V subjected to HIPing. When comparing α phase grain sizes in this study to those of [16], the smaller grain widths encountered in the as-fabricated Ti–6Al–4V can be due to improved fabrication parameters for the processing of this material. The larger average grain width of the α phase observed for HIPed specimens is a result from coarsening due to the thermal treatment utilized. The regular morphology of the Ti–6Al–4V grains suggests no alterations appeared in the microstructure of this material during deposition of copper. Analysis on the copper side revealed that, there was a microstructural change from equiaxed morphology close to the interface to a structure of elongated columnar grains, as reported by [17], with increasing distance from the interface. This effect might be due to the Ti–6Al–4V substrate acting as an epitaxial growth initiator forming equiaxed grains which continue to follow the growth direction. Once some layers of copper had been deposited, this material provided a more effective heat sink that caused a higher thermal flux and provided the conditions for columnar growth or directional solidification [29]. The differences noted in microstructures of as-fabricated multi-material EBM specimens, in particular those of Ti–6Al–4V, are dependent on the conditions used for their fabrication which clearly vary from the regular EBM process in which complete pieces are built in a single machine run. Observations of microstructures in the HIPed specimen show (a) an unaffected acicular microstructure in Ti–6Al–4V, (b) the development of a transition zone in between the joined materials and (c) the presence of twins in copper (Fig. 8). The occurrence of twins has been associated with the grain growth kinetics during heat treatment by annealing of copper [30], suggesting recrystallization of copper occurred during HIPing. The heat treatment also provided coarsening of the α phase grains in the Ti–6Al–4V. The transition zone, that appeared several microns wider compared to the interface

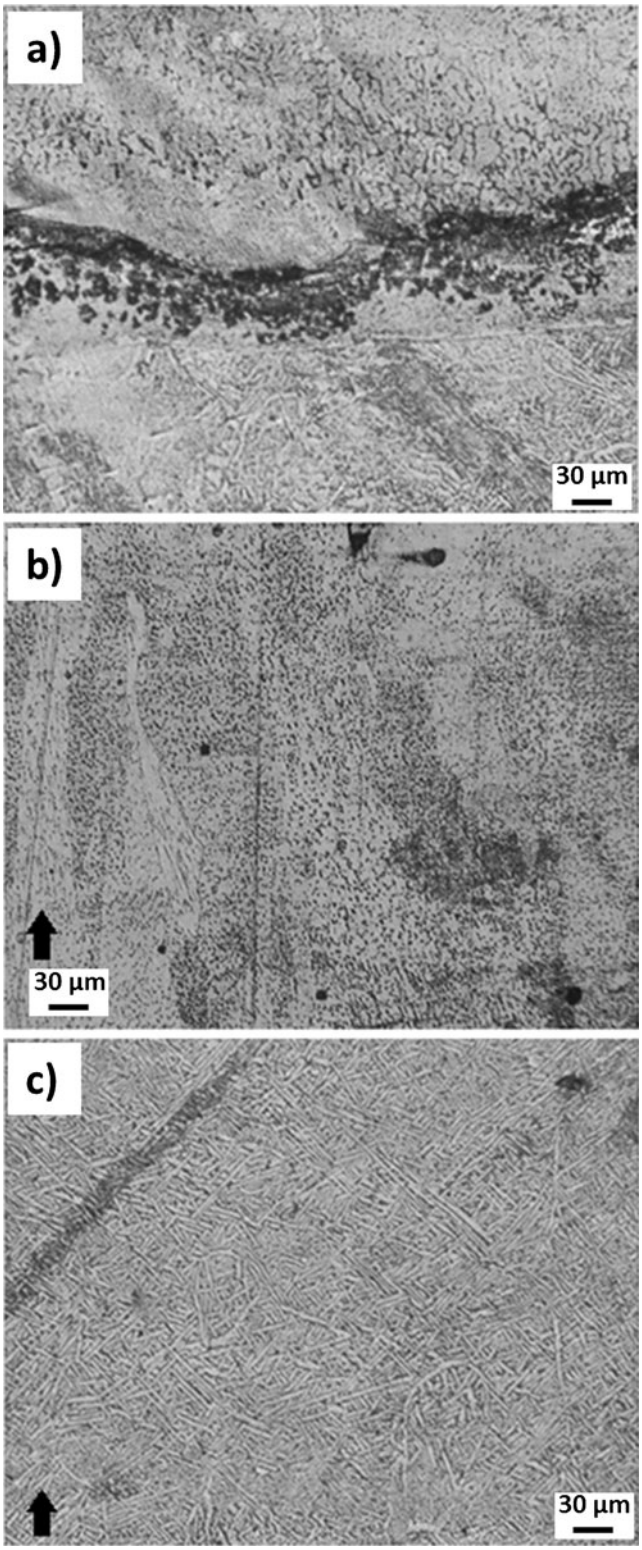

Fig. 7 **a** Interface between Ti–6Al–4V at the bottom and copper on top. **b**, **c** Microstructures observed for copper and Ti–6Al–4V, respectively, in regions away from the interface. *Arrows* indicate the build direction.

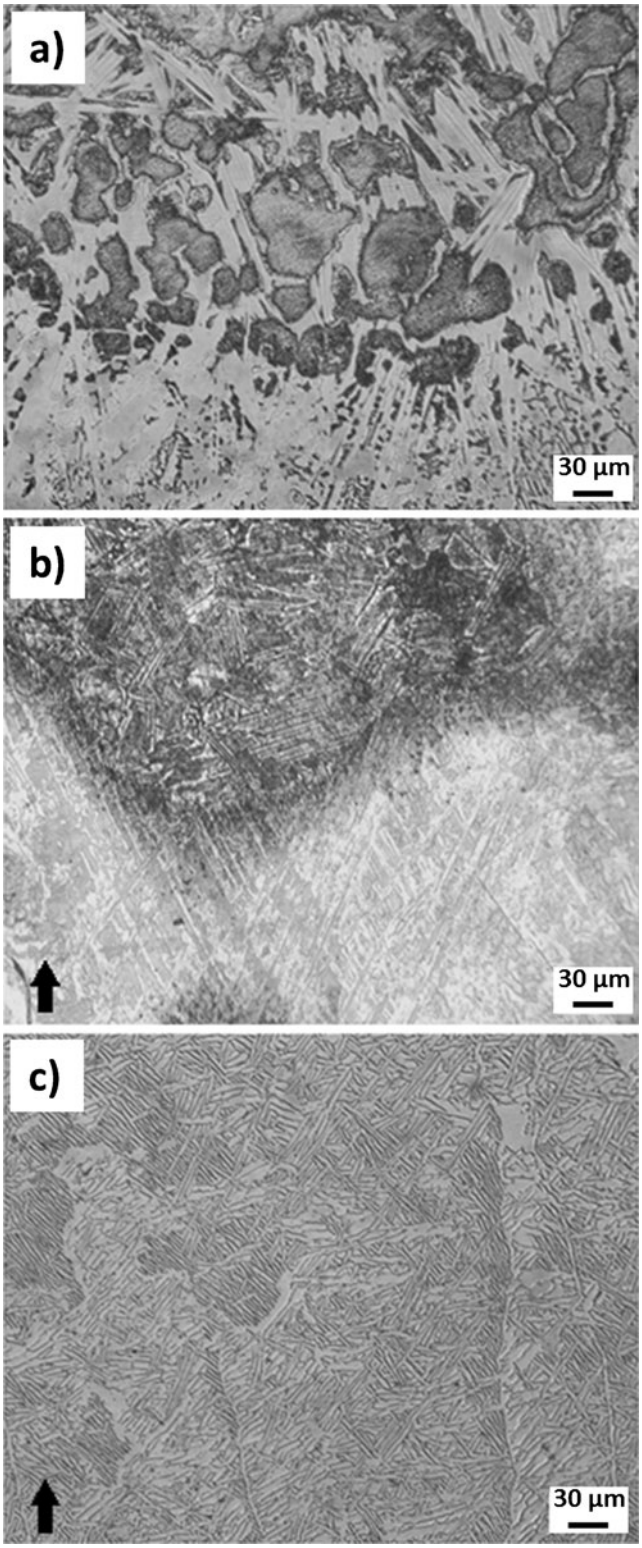

Fig. 8 Microstructures observed in HIPed specimen. **a** Transition zone with different contrast regions, **b** microstructure of copper showing twins, and **c** unaffected Ti–6Al–4V microstructure. *Arrows* indicate the build direction

seen in as-fabricated samples, consisted of regions of diverse contrast (Fig. 8c). Further analysis is needed to reveal if they represent different precipitating phases due to the heat treatment utilized.

3.4 Hardness measurements

The measured Vicker's hardness profiles for as-fabricated and HIPed specimens were plotted for direct comparison (Fig. 9). As a baseline, reported values for EBM processed and annealed Ti–6Al–4V and copper are used for comparison: 350–425 HV for EBM fabricated Ti–6Al–4V [16, 31, 32], 349 HV for annealed Ti–6Al–4V [19], 83–88 HV for EBM fabricated copper [17] and 50 HV for annealed copper [19]. An increase in hardness was observed on the Ti–6Al–4V side near the interface corresponding to 453 HV for the as-fabricated specimen and 476 HV for the HIPed specimen. These values represent an increase of 16 % and 22 %, respectively, over reported values for EBM fabricated Ti–6Al–4V [16, 31]. Curves for both as-fabricated and HIPed Ti–6Al–4V eventually level at ~425 HV away from the interface. More recent studies with Ti–6Al–4V have shown increased values of hardness for the material in the range of 425 HV [33]. On the copper side, hardness values of both as-fabricated and HIPed specimens away from the interface agree with what is reported for the annealed material (50 HV) [20] although the values are below those reported for EBM fabricated copper (83–88 HV) [17]. Close to the interface, the hardness values for copper increased to a range of 150–175 HV. From the plot, it can be inferred that HIPing had the general effect of increasing the hardness of the components. Studies with HIPed copper and parts have reported an associated increase in hardness when compared with non-treated specimens. For instance, HIPed Ti–6Al–4V targets were shown to have higher hardness values and thus better performance against perforation than targets from commercially available Ti–6Al–4V in ballistic tests [34]. Similarly, increased hardness of Ti–6Al–4V powders treated by hot pressing has been observed for different heat treating temperatures [33]. In a study with copper, measured hardness values have been shown to increase in response to applied pressure and temperature during consolidation of bulk copper samples [35]. Because of the complexity of fabrication, only one as-fabricated specimen and one HIPed specimen were utilized for hardness measurements. More specimens need to be fabricated and analyzed to assess the statistical significance of the results.

4 Conclusion

This research demonstrated a methodology for fabricating multi-material metallic components with discrete material regions using current EBM technology. The method was facilitated by the use of a mask start plate that was CNC machined to enable the insertion of Ti–6Al–4V components fabricated during a previous build. The mask start plate with inserted components served as the substrate for the fabrication of copper on top of the Ti–6Al–4V components. The ability for multi-material fabrication was confirmed by the construction of several cylindrical components using Ti–6Al–4V and copper with their long axes oriented in the X and Z directions. The manual registration procedure for alignment of the mask start plate resulted in the components having misalignment values greater than those introduced during the design stage. This indicates the need to improve the registration process between build cycles which will be addressed in future work. The microstructure of Ti–6Al–4V in the as-fabricated EBM and HIPed condition differed from those reported in normal builds of Ti–6Al–4V [16]; a decrease was noted for the width of the α grains in the as-fabricated specimen while a slight increase was observed in this dimension after HIPing. On the copper side, an equiaxed morphology was evident for grains close to the interface and elongated grains away from it. The elongation of grains in EBM fabricated copper has been

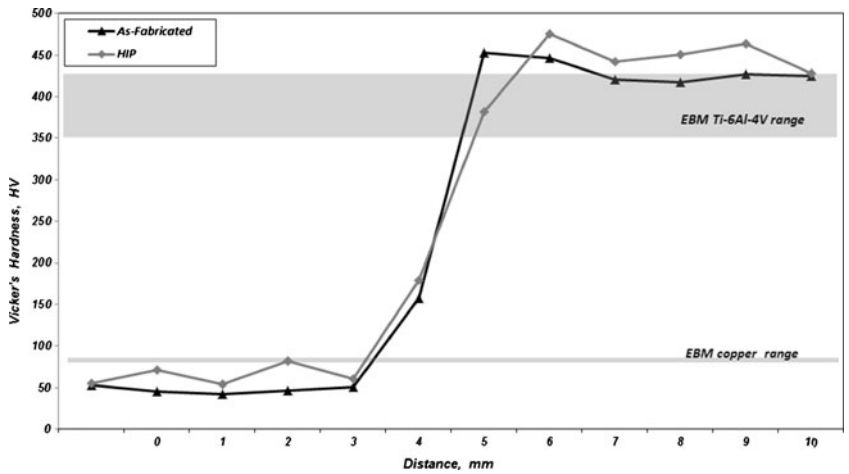

Fig. 9 Hardness profiles obtained for as-fabricated and HIPed samples. Reported ranges for both copper and Ti–6Al–4V processed by EBM are shown for reference

reported before [17]. The initial equiaxed grains might be nucleating in the presence of the Ti–6Al–4V substrate. As far as hardness values, Ti–6Al–4V showed 16 % and 22 % increase for as-fabricated and HIPed, respectively, when compared to published hardness values. Hardness values for the copper in the as-fabricated and HIPed condition remained below reported values for the material when processed by EBM. Differences noted in the microstructure and the hardness of copper and Ti–6Al–4V might be arising due to the processing conditions during the fabrication of multi-material EBM parts, which are very different from to the normal EBM process, when using single materials. Extensions of the methodology presented in this work may become very useful for repair of metallic components because of the advantages offered by EBM processing, and future work could also include EBM fabrication of multi-material parts with graded interfaces. Research is also needed to fully characterize the phases that appear during joining and their effect on the microstructure and bond strength of the interface via mechanical testing of the multi-material components. This research represents the initial steps toward achieving the fabrication of multiple-material metallic components that are able to provide specific spatial properties, resulting in a significant benefit to the desired performance of the component in the particular application. The material combination described in this research can be employed in fabrication of many components for metal extraction, energy production and superconducting devices. Furthermore, extension of this technique can have profound implications, for instance, in the repair of high value components.

Acknowledgements The research presented here was performed at the University of Texas at El Paso (UTEP) within the W.M. Keck Center for 3D Innovation, providing access to state-of-the-art facilities and equipment that have been supported through a variety of sources and most recently through a substantial grant from the State of Texas Emerging Technology Fund. Support was also provided through the endowment from the UTEP Mr. and Mrs. MacIntosh Murchison Chair I in Engineering. The authors are thankful for the participation of undergraduate students Jesus Castro, Jesus Dominguez and David Rodriguez in various aspects of the project.

References

1. American Society for Testing and Materials, Standard F2921-11 (2012) Standard Terminology for Additive Manufacturing–Coordinate Systems and Test Methodologies. ASTM International, West Conshohocken. doi:10.1520/F2921-11
2. American Society for Testing and Materials, Standard F2792-12a (2012) Standard Terminology for Additive Manufacturing Technologies. ASTM International, West Conshohocken. doi:10.1520/F2792-12A
3. Wicker R, MacDonald E (2012) Multi-material, multi-technology stereolithography. Virtual and Physical Prototyping 7(3):181–194
4. Choi J, Kim H, Wicker R (2011) Multi-material stereolithography. Journal of Materials Processing Technology 211:318–328
5. Choi J, MacDonald E, Wicker R (2010) Multi-material microstereolithography. International Journal of Advanced Manufacturing Technology 49:543–551
6. Arcaute K, Mann B, Wicker R (2010) Stereolithography of spatially controlled multi-material bioactive poly(ethylene glycol) scaffolds. Acta Biomaterialia 6:1047–1054
7. Lopes A, MacDonald E, Wicker R (2012) Integrating stereolithography and direct print technologies for 3D structural electronics fabrication. Rapid Prototyping Journal 18:129–143
8. Sigmarsson H, Kinzel E, Chappell W, Xu X (2006) Selective laser sintering of multilayer, multimaterial circuit components. IEEE MTT-S International Microwave Symposium Digest June 2006: 1788–1791
9. Chung H, Das S (2008) Functionally graded nylon-11/silica nanocomposites produced by selective laser sintering. Materials Science and Engineering A-487:251–257
10. Griffith ML, Harwell LD, Romero JT (1997) Multi-material processing by LENS™. Working paper. Sandia National Laboratories
11. Balla V, Xue W, Bose S, Bandyopadhyay A (2008) Functionally graded Co–Cr–Mo coating on Ti–6Al–4V alloy structures. Acta Biomaterialia 4:697–706
12. Balla V, Bandyopadhyay P, Bose S, Bandyipadhyay A (2007) Compositionally graded yttria-stabilized zirconia coating on stainless steel using laser engineered net shaping (LENS™). Scripta Materialia 57:861–864
13. Obielodan J, Stucker B (2010) Dual-material minimum weight structures fabrication using ultrasonic consolidation. In 21st Annual International Solid Freeform Fabrication Symposium, August 2010: 48–81
14. Sun Z, Karppi R (1996) The application of electron beam welding for the joining of dissimilar metals: an overview. Journal of Materials Processing Technology 39:257–267
15. Obielodan J, Ceylan A, Murr L, Stucker B (2010) Multi-material bonding in ultrasonic consolidation. Rapid Prototyping Journal 16: 180–188
16. Murr L, Esquivel E, Quinones S, Gaytan S, Lopez M, Martinez E, Medina F, Hernandez D, Martinez E, Martinez J, Stafford S, Brown D, Hoppe T, Meyers W, Lindhe U, Wicker R (2009) Microstructures and mechanical properties of electron beam-rapid manufactured Ti–6Al–4V biomedical prototypes compared to wrought Ti–6Al–4V. Materials characterization 60:96–105
17. Ramirez D, Murr L, Martinez E, Hernandez D, Martinez J, Machado B, Medina F, Frigola P, Wicker R (2011) Novel precipitate-microstructural architecture developed in the fabrication of solid copper components by additive manufacturing using electron beam melting. Acta Materialia 59:4088–4099
18. Thijs L, Verhaeghe F, Craeghs T, Humbeeck J, Kruth J (2010) A study of the microstructural evolution during selective laser melting of Ti–6Al–4V. Acta Materialia 58:3303–3312
19. MatWeb (2013) Material Property Data. Ti-6Al-4V (Grade 5), Annealed Bar. http://www.matweb.com/search/DataSheet.aspx?MatGUID=10d463eb3d3d4ff48fc57e0ad1037434. Accessed 20 January 2013
20. MatWeb (2013) Material Property Data. Copper, Cu: Annealed. http://matweb.com/search/DataSheet.aspx?MatGUID=9aebe83845c04c1db5126fada6f76f7e. Accessed 20 January 2013
21. Rosa J, Robin A, Silva M, Baldan C, Peres M (2009) Electrodeposition of copper on titanium wires: Taguchi experimental design approach. Journal of Materials Processing Technology 209:1181–1188
22. Demidenko L, Onatskaya N (2008) Solid-state welding of tubular joints of titanium and copper with application of electrohydropulse loading. Surface Engineering and Applied Electrochemistry 44:245–247
23. Kline G, (1983) Titanium clad copper electrode and method for making. U.S. Patent No. 4,411,762
24. Oberg E, Jones F, Horton H, Ryffel H (1996) Machinery's handbook, 25th Edition. New York, USA
25. Engineers Edge (2013) Dowel Pin Tolerance Chart – ASME Y14.5-2009. http://www.engineersedge.com/dowel_pin.htm. Accessed 6 March 2013

26. Froes F, Mashl S, Moxson V, Hebeisen J, Duz V (2004) The technologies of titanium powder metallurgy. JOM: 46–48
27. Teodorescu G (2007) Radiative emissivity of metals and oxidized metals at high temperature. Dissertation, Auburn University
28. Arcam A2 System Technical Data (2013) http://www.arcam.com/CommonResources/Files/www.arcam.com/Documents/Products/Arcam-A2.pdf. Accessed 3 March 2013
29. Versnyder F, Shank M (1970) The development of columnar grain and single crystal high temperature materials through directional solidification. Materials Science and Engineering 6:213–247
30. Field D, Bradford L, Nowell M, Lillo T (2007) The role of annealing twins during recrystallization of Cu. Acta Materialia 55:4233–4241
31. Koike M, Martinez K, Guo L, Chahine G, Kovacevic R, Okabe T (2011) Evaluation of titanium alloy fabricated using electron beam melting system for dental applications. Journal of Materials Processing Technology 211:1400–1408
32. Karlsson J, Snis A, Engqvist H, Lausmaa J (2013) Characterization and comparison of materials produced by Electron Beam Melting (EBM) of two different Ti–6Al–4V powder fractions. Journal of Materials Processing Technology 213:2109–2118
33. Bolzoni L, Montealegre I, Ruiz-Navas E, Gordo E (2012) Microstructural evolution and mechanical properties of the Ti–6Al–4V alloy produced by vacuum hot-pressing. Materials Science and Engineering A-546:189–197
34. Nesterenko V, Goldsmith W, Indrakanti S, Gu Y (2003) Response of hot isostatically pressed Ti–6Al–4V targets to normal impact by conical and blunt projectiles. International Journal of Impact Engineering 28:137–160
35. Srivatsan T, Ravi B, Naruka A, Petraroli M, Kalyanamaran R, Sudarshan T (2002) Influence of consolidation parameters on the microstructure and hardness of bulk copper samples made from nanopowders. Materials and Design 23:291–296